

Topological order in PEPS: Transfer operator and boundary Hamiltonians

Norbert Schuch,^{1,2} Didier Poilblanc,³ J. Ignacio Cirac,⁴ and David Pérez-García⁵

¹*Institut für Quanteninformation, RWTH Aachen, 52056 Aachen, Germany*

²*Institute for Quantum Information, California Institute of Technology, MC 305-16, Pasadena CA 91125, U.S.A.*

³*Laboratoire de Physique Théorique, C.N.R.S. and Université de Toulouse, 31062 Toulouse, France*

⁴*Max-Planck-Institut für Quantenoptik, Hans-Kopfermann-Str. 1, D-85748 Garching, Germany*

⁵*Dpto. Analisis Matemático and IMI, Universidad Complutense de Madrid, E-28040 Madrid, Spain*

We study the structure of topological phases and their boundaries in the Projected Entangled Pair States (PEPS) formalism. We show how topological order in a system can be identified from the structure of the PEPS transfer operator, and subsequently use these findings to analyze the structure of the *boundary Hamiltonian*, acting on the bond variables, which reflects the entanglement properties of the system. We find that in a topological phase, the boundary Hamiltonian consists of two parts: A universal non-local part which encodes the nature of the topological phase, and a non-universal part which is local and inherits the symmetries of the topological model, which helps to infer the structure of the boundary Hamiltonian and thus possibly of the physical edge modes.

The study of strongly correlated quantum systems is of central interest in modern condensed matter physics due to the exciting properties exhibited by those systems, in particular unconventional phases with topological order. In order to identify topological order in such systems, topological entropies [1, 2] have been applied successfully. To obtain more information than contained in the entropy, the entanglement spectrum (ES) – i.e., the spectrum of the reduced density operator of a region – has been studied, and it has been realized that for certain systems, the low-energy part of the ES resembles the spectrum of the thermal state of a one-dimensional (1D) local *boundary Hamiltonian* which can be associated to the boundary of the region studied, and which seems to be related to the physical edge modes of the model [3–6]. While this relation between bulk ES, boundary Hamiltonian, and edge excitations can be made rigorous in some cases [7, 8], in most cases the Hamiltonian is *a posteriori* inferred from the structure of the ES, and a general connection between ES and boundary still needs to be made.

In [9], we made progress in that direction by proving a rigorous connection between ES and boundary using the framework of Projected Entangled Pair States (PEPS) [10], which form the appropriate description of ground states of gapped local Hamiltonians both in conventional and topological phases [11]. This allowed us to derive a one-dimensional boundary Hamiltonian, which we found to be local in trivial phases (without symmetry breaking or topological order). Following the Li-Haldane conjecture about the relation of boundary Hamiltonian and edge physics [3], this allows for conclusions about the structure of a system’s edge excitations. On the other hand, for both symmetry-broken and topological phases we found a highly non-local boundary Hamiltonian, making it impossible to infer something about the actual edge physics. Yet, since this boundary Hamiltonian acts on the virtual bond variables, its local and non-local character are not necessarily reflected in physical space.

In this paper, we establish a framework for studying the boundary Hamiltonian of topologically ordered

phases in the framework of PEPS. We start by showing how topological order is reflected in the properties of the transfer operator, which in turn enables us to decompose the boundary Hamiltonian of topological models into two parts. The *universal part* couples to non-local (topological) degrees of freedom and determines the phase of the system, but is independent on microscopic details. The *non-universal part* is local (thereby generalizing what happens for trivial phases), depends on microscopic details, but vanishes under RG flows; moreover, it commutes with the symmetries which originate from the universal part. Therefore, the non-universal part can help to infer the nature of the edge physics of the model.

Let us first introduce PEPS and explain how to use them to derive boundary theories. For clarity, we restrict to square lattices on a cylinder (with length N_h and circumference N_v). A (translational invariant) PEPS $|\psi\rangle = \sum c_{i_1 \dots i_N} |i_1, \dots, i_N\rangle$ is described by a five-index tensor $A_{\alpha\beta\gamma\delta}^i$ (Fig. 1a, with i the *physical* and $\alpha, \beta, \gamma, \delta$ the *virtual indices*), such that the coefficient $c_{i_1 \dots i_N}$ is obtained by arranging tensors A^{i_1}, \dots, A^{i_N} on the cylinder and contracting each virtual index with the corresponding index of the adjacent tensors, while putting boundary conditions $|\chi_L\rangle, |\chi_R\rangle$ at the open virtual indices at the two ends (Fig. 1c). PEPS naturally appear as ground states of local *parent Hamiltonians* [12, 13]; the boundary conditions $|\chi\rangle$ can be incorporated in the Hamiltonian by making the virtual indices at the boundary physical and including them in the parent Hamiltonian, and additionally acting with a frustration-free Hamiltonian term with ground space $|\chi\rangle$ on them. (In particular, if $|\chi\rangle$ is a Matrix Product State, this Hamiltonian is local.)

As proven in [9] (see also Appendix A), for any PEPS the ES of a half-cylinder (green cut in Fig. 1c) is equal to the spectrum of

$$\sigma \propto \sqrt{\sigma_L^*} \sigma_R \sqrt{\sigma_L^*}, \quad (1)$$

where σ_R is the state obtained at the *virtual indices* of the right half-cylinder by contracting the physical indices with the adjoint, cf. Fig. 1d,f (with $\chi_R = |\chi_R\rangle\langle\chi_R|$,

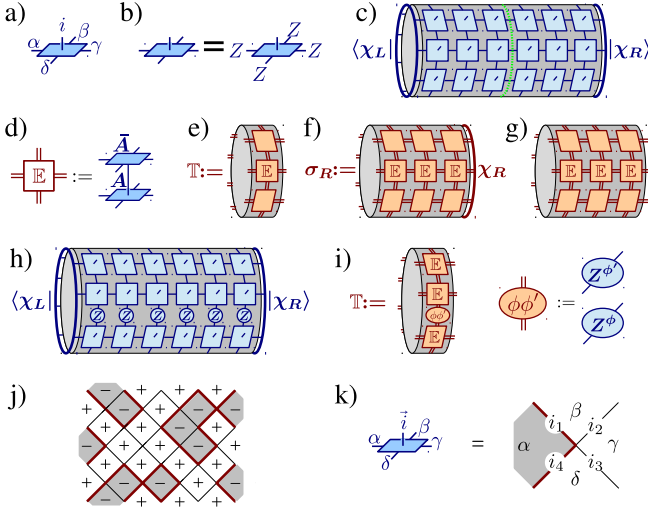


FIG. 1. Tensor networks for entanglement spectra and for topological models; see text for details.

and correspondingly for σ_L); for $N_h \gg 1$, this is just the eigenvector corresponding to the largest eigenvalue of the *transfer operator* \mathbb{T} , Fig. 1d,e. From there, one can construct a *boundary Hamiltonian* $H = -\log \sigma$ which acts on the virtual degrees of freedom at the boundary, and which exactly reproduces the ES. As demonstrated in [9], this Hamiltonian is local if the system is in a trivial phase, and becomes non-local in symmetry broken or topological phases. In this work, we revisit the structure of the boundary Hamiltonian for topological phases: There, the transfer operator exhibits symmetries and degeneracies, giving rise to a non-unique fixed point. As we will show, by properly interpreting the structure of the transfer operator and identifying the physically relevant fixed points, the locality of the boundary Hamiltonian can in part be recovered also for topological phases.

Topological order in PEPS is accompanied by a virtual symmetry of the tensor A , such as the invariance under the representation of a (finite) symmetry group, Fig. 1b [13] (more general symmetries are given, e.g., by Hopf algebras [14] or tensor categories [15]). For simplicity, we focus on \mathbb{Z}_2 symmetry, i.e., A is invariant under $Z^{\otimes 4}$, for some unitary representation $\{\mathbb{1}, Z\}$ of \mathbb{Z}_2 , but our findings easily generalize to any finite group. In that case, the four possible ground states are distinguished by (i) whether $|\chi_L\rangle$ and $|\chi_R\rangle$ are in the ± 1 eigenspace of $Z^{\otimes N_v}$ (i.e., have an even/odd parity of $|1\rangle$'s, denoted $p = e, o$), and (ii) by the possibility of having a string of Z 's along the cylinder, Fig. 1h [13]. It is convenient to picture the Z string as coupled to a flux $\phi \in \{0, \pi\}$ threading the cylinder.

The symmetry Fig. 1b of A induces the same symmetry independently in the ket and bra layer of \mathbb{E} , Fig. 1d, and subsequently in \mathbb{T} (Fig. 1e), i.e., $[\mathbb{T}, Z^{\otimes N_v} \otimes \mathbb{1}^{\otimes N_v}] = [\mathbb{T}, \mathbb{1}^{\otimes N_v} \otimes Z^{\otimes N_v}] = 0$, where the tensor product is w.r.t. ket and bra layer; this is, \mathbb{T} has four blocks corresponding

to the $Z^{\otimes N_v}$ eigenvalue (i.e., parity) for both the ket and the bra layer. If we include the Z string coupled to the flux, Fig. 1h, we find that the overall transfer operator consists of four such transfer operators $\mathbb{T}_\phi^{\phi'}$ (Fig. 1i), each corresponding to a flux ϕ for the ket and ϕ' for the bra layer, respectively. Overall, it follows that the transfer operator is block-diagonal with 16 blocks $\mathbb{T}_{p\phi}^{p'\phi'}$, each corresponding to one of the 16 blocks $\rho_{p\phi}^{p'\phi'}$ ($\rho \equiv \sigma_L, \sigma_R$) of the fixed point density operator, with parity p (p') and flux ϕ (ϕ') on the ket (bra) layer.

As an example, let us consider Kitaev's Toric Code (TC) [16]. Locally, it is a uniform superposition of all closed loops on a lattice, which can be described by assigning dual variables $|\pm\rangle$ (colors) to the plaquettes, with loops wherever the dual variable changes (i.e., loops are boundaries of colored regions), Fig. 1j. The PEPS is then obtained by blocking the marked region and assigning the bonds to the plaquette variables, Fig. 1k. The $Z^{\otimes 4}$ symmetry of the tensor reflects the fact that inverting the entire coloring does not change the state. A Z string along the cylinder (Fig. 1h) flips the coloring, which leads to an odd number of horizontal strings; while an even (odd) $Z^{\otimes N_v}$ parity in $|\chi_L\rangle$ and $|\chi_R\rangle$ gives a state with a plus (minus) superposition of an even and odd number of loops around the cylinder.

For the TC, $\mathbb{E} = (\mathbb{1}^{\otimes 4} + Z^{\otimes 4})$, and thus $\mathbb{T}_\phi^\phi = \frac{1}{2}(\mathbb{1}^{\otimes N_v} \otimes \mathbb{1}^{\otimes N_v} + Z^{\otimes N_v} \otimes Z^{\otimes N_v}) = P_e \otimes P_e + P_o \otimes P_o$, with $P_{e/o} = \frac{1}{2}(\mathbb{1}^{\otimes N_v} \pm Z^{\otimes N_v})$ the projectors onto the even/odd parity subspace at the boundary, while for $\phi' \neq \phi$, $\mathbb{T}_\phi^{\phi'} = 0$. This is, \mathbb{T} has four degenerate fixed points, corresponding to the four “diagonal” blocks $\rho_{p\phi}^{p'\phi'}$ of the boundary. The four blocks correspond to the four ground states, and, as we will see, their degeneracy is essential for the system to be topologically ordered.

To better understand how the structure of the transfer operator reflects the order of the system, we add string tension to the TC, i.e., weigh every configuration with λ^ℓ , where ℓ is the total length of all loops; this can be achieved by locally modifying the tensors (keeping the $Z^{\otimes 4}$ symmetry), and translates to a magnetic field in the Hamiltonian [17, 18]. This model exhibits a topological phase transition at $\lambda_{\text{crit}} = 1/\sqrt{1+\sqrt{2}} \approx 0.644$ (with $\lambda = 1$ the TC and $\lambda = 0$ the vacuum) [17].

Fig. 2a shows the modulus of the largest eigenvalue $\gamma_{p\phi}^{p'\phi'}$ for each block $\mathbb{T}_{p\phi}^{p'\phi'}$ of the transfer operator. We first focus on the topological phase: We find that the four “diagonal” blocks $\mathbb{T}_{p\phi}^{p\phi}$ are essentially degenerate (the splitting vanishes exponentially with N_v , see Fig. 2b), which ensures that there are four stable ground states. At the same time, the off-diagonal blocks are strictly smaller than the diagonal blocks, which ensures that the four states are linearly independent in the thermodynamic limit (see later). In addition, we find that the diagonal blocks $\mathbb{T}_{p\phi}^{p\phi}$ are gapped (not shown), which ensures that each block has a unique fixed point $\rho_{p\phi}^{p\phi}$.

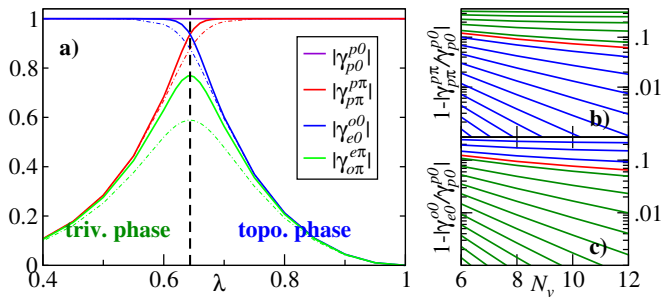


FIG. 2. **a)** Maximal eigenvalues $\gamma_{p\phi}^{p'\phi}$ for the TC with string tension (relative to γ_{e0}^{e0}) for $N_v = 12$ (solid lines) and $N_v = 6$ (dash-dotted lines). **b,c)** Splitting $1 - |\gamma_{p\pi}^{p\pi}/\gamma_{p0}^{p0}|$ (**b**) and $1 - |\gamma_{e0}^{o0}/\gamma_{p0}^{p0}|$ (**c**) for $\lambda = 0.65, 0.66, \dots$ (blue, topological phase), and $\lambda = 0.64, 0.63, \dots$ (green, trivial phase). The red line is $\lambda = 0.644 \approx \lambda_{\text{crit}}$. The calculations (as well as the ones in Figs. 3 and 4) have been carried out using exact column-wise contraction (cf. [9, 19, 20]) and are thus exact.

Altogether, we find that the fixed point of the transfer operator is a direct sum of the $\rho_{p\phi}^{p\phi}$ (i.e., block-diagonal), with weights determined by the boundary condition $|\chi\rangle$. Symmetrizing, Eq. (1), preserves this block structure, and we find that the density operator σ_{topo} which reproduces the ES is of the form

$$\sigma_{\text{topo}} = w_{e0}^{e0} \sigma_{e0}^{e0} \oplus w_{o0}^{o0} \sigma_{o0}^{o0} \oplus w_{e\pi}^{e\pi} \sigma_{e\pi}^{e\pi} \oplus w_{o\pi}^{o\pi} \sigma_{o\pi}^{o\pi}, \quad (2)$$

where the weights $w_{p\phi}^{p\phi} \geq 0$ can be adjusted arbitrarily by appropriate boundary conditions. We can now define a Hamiltonian $H = -\log \sigma$ which reproduces the ES. H commutes with both Z parity and flux, this is, there are H_ϕ , $\phi = 0, \pi$, satisfying $[H_\phi, Z^{\otimes N_v}] = 0$, i.e., the H_ϕ obey a superselection rule inherited from the topological symmetry.

Hamiltonians with different weights $w_{p\phi}^{p\phi}$ (H_ϕ) and $q_{p\phi}^{p\phi}$ (H'_ϕ) are related via $H'_\phi = H_\phi - \log(q_{e\phi}^{e\phi}/w_{e\phi}^{e\phi}) P_e \oplus \log(q_{o\phi}^{o\phi}/w_{o\phi}^{o\phi}) P_o$. This implies two things: First, the boundary Hamiltonians obtained for different boundary conditions differ just by a *universal* contribution which only depends on the underlying symmetry but not on microscopic details. Second, since $P_{e/o} = \frac{1}{2}(\mathbb{1}^{\otimes N_v} \pm Z^{\otimes N_v})$, the boundary Hamiltonian will generally be highly non-local, and, if at all, will only be local for a specific choice $w_{p\phi}^{p\phi}$.

As discussed in Appendix B, the only choice for which we can expect a local Hamiltonian is $w_{e\phi}^{e\phi} = w_{o\phi}^{o\phi}$. The result for the TC with string tension is shown in Fig. 3, and we find indeed that the terms in H_ϕ decay exponentially with distance, i.e., H_ϕ is local (see Appendix C). Note that by combining the locality of H_ϕ with the symmetry $[H_\phi, Z^{\otimes N_v}] = 0$, we can already infer that H_ϕ must be well approximated by a parity preserving nearest neighbor Hamiltonian; in the language of creation/annihilation operators, this amounts to hopping, pairing, repulsion, and on-site potential terms. Closer

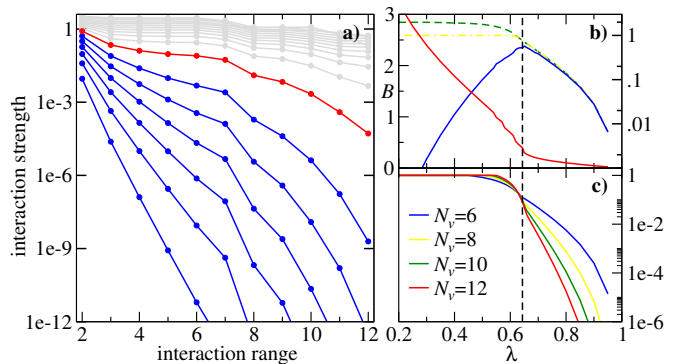


FIG. 3. **a)** Interaction range of H_0 for the TC with string tension ($N_v = 12$), obtained using Eq. (2) with equal weights, which is the correct interpretation for the topological sector. Interactions in the topological phase (blue, $\lambda = 0.7, 0.75, \dots$) decay exponentially. In the trivial phase (grey, $\lambda = 0.60, 0.55, \dots$), the interpretation is no longer valid, seemingly leading to a non-local Hamiltonian. (The red line is λ_{crit} .) **b)** By changing to the interpretation of the transfer operator which is valid in the trivial phase (see text), we obtain a H_0 which is local in the trivial phase. The blue line shows $\|\sigma_{\text{triv}} - \mu(B)\|_1/N_v$ for $N_v = 12$ (right scale), cf. text, and the red line the corresponding B (left scale). The comparison with $\|\sigma_{\text{triv}} - \mu(B=0)\|_1/N_v$ (green) and $\|\sigma_{\text{topo}} - \mu(B)\|_1/N_v$ [yellow, cf. Eq. (2)], shows that the boundary Hamiltonian is well approximated by $B \sum X_i$ in the trivial phase, while the decay in the topological phase is due to the high temperature. **c)** Comparison of H_0 and H_π . The plot shows $\|H_0 - \mathcal{F}(H_\pi)\|_{\text{op}}/\|H_0 - H_\pi\|_{\text{op}}$, where \mathcal{F} flips the sign of all terms which change the parity across the boundary (see text); in the topological phase, the difference converges to 0 exponentially in N_v .

analysis yields that H_ϕ is very well approximated by an Ising Hamiltonian $\sum X_i X_{i+1}$, with strongly suppressed longer-range Ising couplings, and even more strongly suppressed many-body terms. One would naturally expect that H_0 and H_π only differ by a phase $e^{i\pi} = -1$ for terms which change the parity across the boundary, which is indeed what we observe (Fig. 3c).

Figure 3 also shows that H_ϕ becomes long-ranged at the phase transition and stays so in the trivial phase, seemingly contradicting earlier findings [9] where the Hamiltonian in the trivial phase was local. However, the derivation of H_ϕ was based on the structure of the transfer operator, which changes radically in the trivial phase (Fig. 2): First, eigenvalues corresponding to $\phi = \pi$, $\gamma_{p\pi}^{p\pi}$, become strictly smaller than one. This implies that the norm of states in the $\phi = \pi$ sector vanishes exponentially in N_h , and thus, states in that sector are unstable: Any random symmetry-preserving perturbation of A (and thus of the parent Hamiltonian) will yield an admixture of the $\phi = 0$ sector at N_v th order, and thus, for an appropriate ratio N_v/N_h , the $\phi = \pi$ sector vanishes in the thermodynamic limit. It remains to see what happens to the two states in the $\phi = 0$ sector. There, $|\gamma_{e0}^{o0}| \rightarrow \gamma_{e0}^{e0} = \gamma_{o0}^{o0}$ (see Fig. 2c), which im-

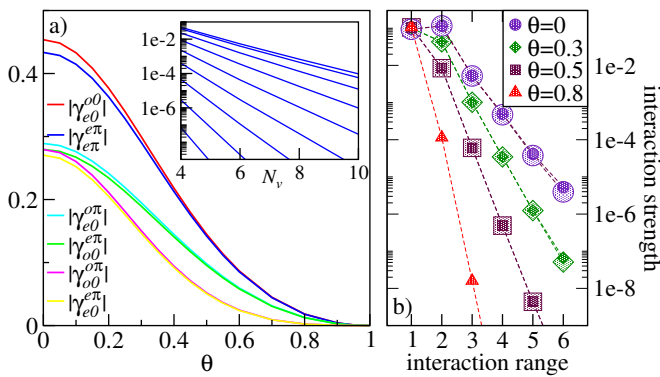


FIG. 4. RVB–TC interpolation. **a)** $|\gamma_{p\phi}^{p'\phi'}|$ for the off-diagonal blocks as a function of the interpolation parameter θ (with $\theta = 0$ the RVB, and $\theta = 1$ the TC), with normalization $\gamma_{e0}^{e0} = 1$, for $N_v = 10$. Inset: Maximal splitting of the diagonal blocks $|\gamma_{p\phi}^{p\phi}|$ (from top: $\theta = 0, 0.1, 0.2, \dots$). **b)** Interaction range along the interpolation for $N_v = 6, 8$ (small/large symbols).

plies that the two states in this sector become equal in the thermodynamic limit, since their overlap is given by $\text{tr}[\mathbb{T}_{e0}^{\sigma 0}] / \sqrt{\text{tr}[\mathbb{T}_{e0}^{\sigma 0}] \text{tr}[\mathbb{T}_{o0}^{\sigma 0}]} \rightarrow (\gamma_{e0}^{e0} / \sqrt{\gamma_{e0}^{e0} \gamma_{o0}^{o0}})^{N_h} \rightarrow 1$. Thus, studying the transfer operator reveals that the system in fact has only one ground state.

In accordance with the changed structure of the transfer operator in the trivial phase, the boundary state σ_{triv} can be any state $\sigma_{\text{triv}} = \sum_{p,p'} w_{p0}^{p'0} \sigma_{p0}^{p'0} \geq 0$, which all have the same spectrum but yield different Hamiltonians. Choosing $w_{e0}^{e0} = w_{o0}^{o0} = \frac{1}{2}$ and extremal $w_{e0}^{o0} = w_{o0}^{e0}$ (such that σ_{triv} becomes singular), we find that σ_{triv} is well approximated by $\mu(\beta) = \exp[-B \sum X_i] / Z$, see Fig. 3b.

Let us briefly summarize our findings: We have found that the virtual symmetry of topological PEPS (Fig. 1b) induces a block-diagonal structure of the transfer operator; topological order is witnessed by the degeneracy of the diagonal blocks. We can then construct boundary Hamiltonians $H'_\phi = \beta_{\text{topo}} H_{\text{topo}} + H_\phi$, with a *universal part* $H_{\text{topo}} = Z^{\otimes N_v}$ which only depends on the symmetry (which is universal), and a β_{topo} which depends on the boundary conditions. The *non-universal part* H_ϕ is local (i.e., vanishes under RG) and thus represents the short-range physics of the system, and it is independent of boundary conditions. A phase transition is accompanied by a diverging interaction length of H_ϕ . H_ϕ inherits the PEPS symmetry, $[H_\phi, Z^{\otimes N_v}] = 0$, which – together with the locality of H_ϕ – allows to infer much of its structure, and it couples to the flux in a natural way. Note that the symmetry also constrains the structure of the physical edge modes: The space of zero-energy excitations is spanned by putting arbitrary boundary conditions

$|b\rangle$ with $\langle b|e^{-H}|b\rangle > 0$ at the open bonds, which restricts them to $Z^{\otimes N}|b\rangle = |b\rangle$.

Our findings generalize straightforwardly to cylinders with two virtual boundaries, Fig. 1g, as encountered when studying the ES on a torus. From the form of the transfer operator, it is immediate that $H'_\phi = \beta_{\text{topo}}(P_{\text{even}} \otimes P_{\text{even}} + P_{\text{odd}} \otimes P_{\text{odd}}) + H_\phi \otimes \mathbb{1} + \mathbb{1} \otimes H_\phi$, where $\beta_{\text{topo}} = \infty$ (i.e., the total parity must be even), and where the non-universal H_ϕ is the same as before. (H_ϕ can differ for the two boundaries if \mathbb{T} is not hermitian.) The form of the boundary has also consequences for the topological entropy $S(\rho_L) = S(\sigma) = \mathcal{H}(\{w_{p\phi}^{p\phi}\}) + \sum w_{p\phi}^{p\phi} S(\sigma_{p\phi}^{p\phi})$, with $\mathcal{H}(\cdot)$ the Shannon entropy: Depending on the boundary conditions, $\mathcal{H}(\{w_{p\phi}^{p\phi}\})$ changes and thus the topological correction varies between 1 and -1 . Note that our findings generalize to any finite group, where the blocks of the transfer operator are labelled by the particle types of the model [16].

We have applied our findings to the Resonating Valence Bond (RVB) state on the kagome lattice, and an interpolation from it to the TC, see Appendix D and [19]. The tensors for the RVB have a \mathbb{Z}_2 symmetry with representation $Z = \text{diag}(1, 1, -1)$; additionally, there is an $\text{SU}(2)$ symmetry with representation $\frac{1}{2} \oplus 0$. Thus, we expect the boundary Hamiltonian to describe a system with a spinful particle or vacuum per site, with $\text{SU}(2)$ invariance and conserved particle parity – similar to a t - J model, but without particle number conservation. Fig. 4a shows the spectrum of the transfer operator for the RVB–TC interpolation: The four “diagonal” blocks are essentially degenerate (inset), while the off-diagonal blocks are suppressed, witnessing topological order in the system. The boundary Hamiltonian H_0 is local throughout, see Fig. 4b; with dominant hopping and smaller repulsion and Heisenberg terms at the RVB point. These results provide further evidence that the RVB is in the same phase as the TC, and that its edge physics resembles a bosonic t - J model.

Acknowledgements.—We acknowledge helpful discussions with F. Verstraete. NS acknowledges support by the Alexander von Humboldt foundation, the Caltech Institute for Quantum Information and Matter (an NSF Physics Frontiers Center with support of the Gordon and Betty Moore Foundation) and the NSF Grant No. PHY-0803371. DP acknowledges support by the Agence Nationale de la Recherche under grant No. ANR 2010 BLANC 0406-0, and CALMIP (Toulouse) for super-computer resources. JIC acknowledges support by the EU project AQUITE, the DFG SFB 631 and Exzellenzcluster NIM, and Catalunya Caixa. DP-G acknowledges QUEVADIS and Spanish grants QUITEMAD and MTM2011-26912.

[1] A. Kitaev and J. Preskill, Phys. Rev. Lett. **96**, 110404 (2006), hep-th/0510092.

[2] M. Levin and X.-G. Wen, Phys. Rev. Lett. **96**, 110405 (2006), cond-mat/0510613.

- [3] H. Li and F. D. M. Haldane, Phys. Rev. Lett. **101**, 010504 (2008), arXiv:0805.0332.
- [4] D. Poilblanc, Phys. Rev. Lett. **105**, 077202 (2010), arXiv:1005.2123.
- [5] A. M. Läuchli and J. Schliemann, Phys. Rev. B **85**, 054403 (2012), arXiv:1106.3419.
- [6] J. Schliemann, Phys. Rev. B **83**, 115322 (2011), arXiv:1008.5289.
- [7] L. Fidkowski, (2009), arXiv:0909.2654.
- [8] X.-L. Qi, H. Katsura, and A. W. W. Ludwig, Phys. Rev. Lett. **108** (2012), arXiv:1103.5437.
- [9] J. I. Cirac, D. Poilblanc, N. Schuch, and F. Verstraete, Phys. Rev. B **83**, 245134 (2011), arXiv:1103.3427.
- [10] F. Verstraete and J. I. Cirac, (2004), cond-mat/0407066.
- [11] M. B. Hastings, Phys. Rev. B **76**, 035114 (2007), cond-mat/0701055.
- [12] D. Perez-Garcia, F. Verstraete, J. I. Cirac, and M. M. Wolf, Quantum Inf. Comput. **8**, 0650 (2008), arXiv:0707.2260.
- [13] N. Schuch, I. Cirac, and D. Pérez-García, Ann. Phys. **325**, 2153 (2010), arXiv:1001.3807.
- [14] O. Buerschaper, J. M. Mombelli, M. Christandl, and M. Aguado, (2010), arXiv:1007.5283.
- [15] M. A. Levin and X.-G. Wen, Phys. Rev. B **71**, 045110 (2005), cond-mat/0404617.
- [16] A. Kitaev, Ann. Phys. **303**, 2 (2003), quant-ph/9707021.
- [17] C. Castelnovo and C. Chamon, Phys. Rev. B **77**, 054433 (2008), arXiv:0707.2084.
- [18] S. Trebst, P. Werner, M. Troyer, K. Shtengel, and C. Nayak, Phys. Rev. Lett. **98**, 070602 (2007), cond-mat/0609048.
- [19] N. Schuch, D. Poilblanc, J. I. Cirac, and D. Pérez-García, Phys. Rev. B **86**, 115108 (2012), arXiv:1203.4816.
- [20] D. Poilblanc, N. Schuch, D. Pérez-García, and J. I. Cirac, Phys. Rev. B **86**, 014404 (2012), arXiv:1202.0947.
- [21] M. B. Hastings, Phys. Rev. B **73**, 085115 (2006), cond-mat/0508554.
- [22] V. Elser and C. Zeng, Phys. Rev. B **48**, 13647 (1993).
- [23] C. Nayak and K. Shtengel, Phys. Rev. B **64**, 064422 (2001), cond-mat/0010242.

Appendix A: Entanglement spectrum for PEPS

In this Appendix, we explain how to derive Eq. (1) for the entanglement spectrum, cf. Ref. [9]. Consider a bipartition of a PEPS into a left and a right part, and denote the physical indices i_1, \dots, i_{N_L} in the left part by $\mathbf{i} = (i_1, \dots, i_{N_L})$, and the physical indices i_{N_L+1}, \dots, i_N in the right part by $\mathbf{j} = (i_{N_L+1}, \dots, i_N)$. Further denote the virtual indices $\alpha_1, \dots, \alpha_{N_v}$ crossing the boundary by $\boldsymbol{\alpha} = (\alpha_1, \dots, \alpha_{N_v})$. Then, the total state can be written as

$$|\Psi\rangle = \sum_{\boldsymbol{\alpha}} L_{\boldsymbol{\alpha}\mathbf{i}} R_{\boldsymbol{\alpha}\mathbf{j}} |\mathbf{i}\rangle |\mathbf{j}\rangle,$$

where $L_{\boldsymbol{\alpha}\mathbf{i}}$ and $R_{\boldsymbol{\alpha}\mathbf{j}}$ are obtained by contracting all tensors in the left and right half, respectively. We define $\sigma_L = LL^\dagger$ and $\sigma_R = RR^\dagger$, as discussed just before Eq. (1); moreover, we introduce the polar decomposition of L , $L = PV$, where V is an isometry and

$P = \sqrt{LL^\dagger} = \sigma_L$. Then, the reduced state of $|\Psi\rangle$ on the left is

$$\begin{aligned} \rho_L &= \sum_{\mathbf{i}, \mathbf{i}'} \sum_{\boldsymbol{\alpha}, \boldsymbol{\alpha}'} L_{\boldsymbol{\alpha}\mathbf{i}} R_{\boldsymbol{\alpha}'\mathbf{i}'} L_{\boldsymbol{\alpha}'\mathbf{i}}^* R_{\boldsymbol{\alpha}\mathbf{i}'}^* |\mathbf{i}\rangle \langle \mathbf{i}'| \\ &= L^T R R^\dagger L^* \\ &= V^T \sqrt{\sigma_L^*} \sigma_R \sqrt{\sigma_L} V^*. \end{aligned}$$

Since V is an isometry, it follows that ρ_L and $\sigma = \sqrt{\sigma_L^*} \sigma_R \sqrt{\sigma_L}$ have the same spectrum, which proves Eq. (1).

Appendix B: Asymptotic equiprobability of parity blocks in the Gibbs state

In this Appendix, we give a partial proof for the following Conjecture, which proves that in order to obtain a local boundary Hamiltonian, the weight of the states in all sectors has to be chosen equal.

Conjecture 1 *Let $H = \sum_{i=1}^N h_i$ be a Hamiltonian on a chain of d -level systems of length N with periodic boundaries, such that $\|h_i\| \leq 1$, and each of the h_i has interaction range at most k . Further, there exists a single-site operator Z with eigenvalues ± 1 such that $[h_i, Z^{\otimes N}] = 0$ for all i . Then,*

$$\lim_{N \rightarrow \infty} \frac{\text{tr}[Z^{\otimes N} e^{-\beta H}]}{\text{tr}[e^{-\beta H}]} = 0$$

for any $0 \leq \beta < \infty$.

For sufficiently small β , the conjecture can be proven using a result of Hastings [21]. There, it is shown that for some $\beta < \beta^* = O(1)$ (which depends on the lattice geometry), $\exp[-\beta H]$ can be approximated up to an error $\epsilon = \exp[N \exp(-\ell/\xi)] - 1$ in trace norm by a mixture

$$\rho(\ell) = \sum_A p_A \bigotimes_{A \in A} \rho_A,$$

where the sum goes over partitions $\mathcal{A} = (A_1, A_2, \dots)$ of the chain into blocks A_i of length at most ℓ , the ρ_A are Gibbs states on block A , and ξ is a constant depending on the lattice geometry. By choosing $\ell = (1 + \kappa)\xi \log N$ ($\kappa > 0$), we find that $\epsilon = \exp[N^{-\kappa}] - 1 \leq 2N^{-\kappa} \rightarrow 0$.

On the other hand, we can bound

$$\left| \frac{\text{tr}[Z^{\otimes |A|} \rho_A]}{\text{tr}[\rho_A]} \right| \leq \frac{e^{\beta\ell} - e^{-\beta\ell}}{e^{\beta\ell} + e^{-\beta\ell}} = \tanh(\beta\ell),$$

and thus

$$\begin{aligned} \left| \frac{\text{tr}[Z^{\otimes N} \rho(\ell)]}{\text{tr}[\rho(\ell)]} \right| &\leq \tanh(\beta\ell)^{N/\ell} \\ &\leq (1 - \exp[-2\beta\ell])^{N/\ell} \\ &= (1 - N^{-2\beta(1+\kappa)\xi})^{N/\ell} \end{aligned}$$

For large enough N , we can further bound $N/\ell \geq N^{1-\delta}$ for any $\delta > 0$, and thus (with $M = N^{1-\delta}$)

$$\left| \frac{\text{tr}[Z^{\otimes N} \rho(\ell)]}{\text{tr}[\rho(\ell)]} \right| \leq \left[1 - M^{-\frac{2\beta(1+\kappa)\xi}{1-\delta}} \right]^M \rightarrow 0$$

as long as $2\beta(1+\kappa)\xi/(1-\delta) < 1$, i.e., as long as

$$\beta < \tilde{\beta} = \frac{1}{2(1+\kappa)\xi}.$$

Combining this with the bound on the trace norm distance between the Gibbs state and $\rho(\ell)$, this proves the conjecture for sufficiently small β .

Appendix C: Analysis of the locality of the boundary Hamiltonian

In this Appendix, we explain how we determine the locality of the Hamiltonian by decomposing it into local terms, as shown in Figs. 3 and 4.

Given a Hamiltonian H on N spins, we can decompose it as

$$H = \sum_{i_1, \dots, i_N=0}^3 c_{i_1, \dots, i_N} \sigma^{i_1} \otimes \sigma^{i_2} \otimes \dots \otimes \sigma^{i_N},$$

where $\sigma^0, \sigma^1, \sigma^2, \sigma^3 = \mathbb{1}, X, Y, Z$ are the Pauli matrices. Any term in the sum is characterized by a string (i_1, \dots, i_N) ; we say it has locality d if the maximal distance (with periodic boundaries) of any two $i_k \neq 0$ is d . (Thus, $d = 0$ are one-site terms, $d = 1$ are nearest neighbor terms, $d = 2$ includes both next-nearest neighbor two-body terms and true three-body terms on three contiguous spins, etc.)

The plots show the overall weight of terms with locality d as a function of d , i.e., $w_d = |\vec{c}_d|$, where \vec{c}_d is the vector of all c_{i_1, \dots, i_N} with locality d , and $|\cdot|$ is the 2-norm. By choosing the 2-norm, we ensure that w_d is independent of the choice of local basis (with operator-norm normalized basis elements). This can be seen by noting that for hermitian single-site operator, $O = \alpha\sigma^1 + \beta\sigma^2 + \gamma\sigma^3$, $\|O\|_\infty = \sqrt{\alpha^2 + \beta^2 + \gamma^2}$, i.e., rotationally invariant and thus basis-independent.

Appendix D: RVB and PEPS

For the convenience of the reader, we provide here a brief introduction to Resonating Valence Bond (RVB) states in the PEPS formalism, as well as the interpolation from it to the Toric Code. We refer the reader interested in more details to Ref. [19].

Let us first introduce the dimer and resonating valence bond (RVB) states on the kagome lattice. A *dimer* is a pair of vertices connected by an edge. A *dimer covering* is a complete covering of the lattice with dimers, Fig. 5a. We can associate orthogonal quantum states $|D\rangle$ with each dimer covering D . Then, the *dimer state* is given by

the equal weight superposition $|\Psi_{\text{dimer}}\rangle = \sum |D\rangle$, where the sum runs over all dimer coverings D . Note that the dimer state is known to be locally unitarily equivalent to Kitaev's Toric Code [19, 22, 23].

To obtain the RVB state, we now associate to each vertex of the lattice a spin- $\frac{1}{2}$ particle with basis states $|0\rangle \equiv |\uparrow\rangle$ and $|1\rangle \equiv |\downarrow\rangle$. Then, for each dimer covering D we define a state $|\sigma(D)\rangle$ which is a tensor product of singlets $|01\rangle - |10\rangle$ (we omit normalization throughout) between the pairs of spins in each dimer in the covering (using some consistent orientation). The *resonating valence bond* (RVB) state is then defined as the equal weight superposition $|\Psi_{\text{RVB}}\rangle = \sum_D |\sigma(D)\rangle$ over all dimer coverings.

To obtain a PEPS description of the RVB state, we first place 3-qutrit states

$$|\varepsilon\rangle = \sum_{i,j,k=0}^2 \varepsilon_{ijk} |ijk\rangle + |222\rangle, \quad (\text{D1})$$

inside each triangle of the kagome lattice, as depicted in Fig. 5b. Here, ε_{ijk} is the completely antisymmetric tensor with $\varepsilon_{012} = 1$, and i, j , and k are oriented clockwise. This corresponds to having either one or no singlet in the $\{|0\rangle, |1\rangle\}$ subspace in the triangle, the absence of a singlet being marked by $|2\rangle$. Second, we apply the map

$$\mathcal{P} = |0\rangle(\langle 02| + \langle 20|) + |1\rangle(\langle 12| + \langle 21|) \quad (\text{D2})$$

at each vertex, which selects exactly one singlet per vertex. It is straightforward to check that this construction exactly gives the RVB state. If we replace \mathcal{P} by

$$\mathcal{P}_\perp = |02\rangle\langle 02| + |12\rangle\langle 12| + |20\rangle\langle 20| + |21\rangle\langle 21|, \quad (\text{D3})$$

we obtain a representation of the dimer state, since now all dimer configurations are locally orthogonal. Finally, we can smoothly interpolate between the dimer and the RVB (up to isometry), by choosing

$$\begin{aligned} \mathcal{P}(\theta) = & |+\rangle \left[|0\rangle(\langle 02| + \langle 20|) + |1\rangle(\langle 12| + \langle 21|) \right] \\ & + \theta |-\rangle \left[|0\rangle(\langle 02| - \langle 20|) + |1\rangle(\langle 12| - \langle 21|) \right], \end{aligned} \quad (\text{D4})$$

with $\theta = 1$ the dimer and $\theta = 0$ the RVB state, which is the interpolation studied in Fig. 4.

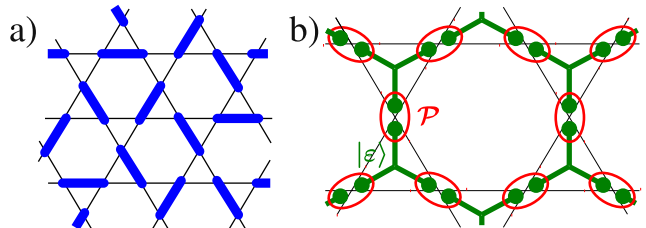


FIG. 5. **a)** Dimer covering of the kagome lattice. **b)** PEPS construction for the RVB state on the kagome lattice.